

Why epithelial cells collectively move against a traveling signal wave

Tatsuya Fukuyama,^{1,2} Hiroyuki Ebata,^{1,3} Akihisa Yamamoto,^{4,5} Ryo Ienaga,^{1,2} Yohei Kondo,^{6,7,8,9} Motomu Tanaka,^{4,10} Satoru Kidoaki,³ Kazuhiro Aoki,^{6,7,8,9,11} and Yusuke T. Maeda^{1,2,*}

¹Department of Physics, Kyushu University, Fukuoka 819-0395, Japan

²Department of Chemical Engineering, Kyoto University, Kyoto 615-8246, Japan

³Institute for Materials Chemistry and Engineering, Kyushu University, Fukuoka 819-0395, Japan

⁴Center for Integrative Medicine and Physics, Institute for Advanced Study, Kyoto University, Kyoto 606-8501, Japan

⁵RIKEN Interdisciplinary Theoretical and Mathematical Sciences Program (iTHEMS), Wako, Saitama 351-0198, Japan

⁶National Institute for Basic Biology, NINS, Aichi 444-8787, Japan

⁷ExCELLS, NINS, Aichi 444-8787, Japan

⁸Department of Basic Biology, SOKENDAI, Aichi 444-8787, Japan

⁹Laboratory of Cell Cycle Regulation, Graduate School of Biostudies, Kyoto University, Kyoto 606-8501, Japan

¹⁰Physical Chemistry of Biosystems, Institute of Physical Chemistry, Heidelberg University, D69120 Heidelberg, Germany

¹¹Center for Living Systems Information Science (CeLiSIS), Graduate School of Biostudies, Kyoto University, Kyoto 606-8501, Japan

(Dated: February 21, 2025)

The response of cell populations to external stimuli plays a central role in biological mechanical processes such as epithelial wound healing and developmental morphogenesis. Wave-like propagation of a signal of ERK MAP kinase has been shown to direct collective migration in one direction; however, the mechanism based on continuum mechanics under a traveling wave is not fully understood. To elucidate how the traveling wave of the ERK kinase signal directs collective migration, we constructed the mechanical model of the epithelial cell monolayer by considering the signal-dependent coordination of contractile stress and cellular orientation. The proposed model was studied by using an optogenetically-controlled cell system where we found that local signal activation induces changes in cell density and orientation with the direction of propagation. The net motion of the cell population occurred relative to the wave, and the migration velocity showed a maximum in resonance with the velocity of the ERK signal wave. The presented mechanical model was further validated in *in vitro* wound healing process.

I. INTRODUCTION

Collective migration refers to the cohesive motion of cells as a group, exhibiting a high degree of correlation in migration direction [1]. The cells align their direction of movement through cell adhesion to one another, thereby enabling the group of cells to move in a coordinated fashion. These collective cell migrations play essential roles in tissue remodeling processes *in vivo*, as evidenced by the observation of embryonic development, wound healing of epithelial tissues, and cancer cell invasion [1–5]. *In vitro* wound healing assay with cultured epithelial cells such as MDCK cells has been widely used as a model system for collective migration. Recent studies reveal that the direction of collective migration during *in vitro* wound healing is regulated by intracellular signaling pathways [6]. The extracellular signal-regulated kinase (ERK) pathway is a representative model in this regard [2]; the ERK MAP kinase is an intracellular signal transduction protein known to regulate cell proliferation, differentiation, migration, and apoptosis [7]. During collective migration of epithelial monolayer cells, the ERK activity transiently increases in cells in the vicinity of the injured region. As ERK activity is upregulated in the

cells, the ERK activation causes EGFR-ligand cleavage in those cells and subsequent the activation of EGFR-Ras-ERK pathway in the neighboring cells, leading to the propagation of ERK activation as a trigger wave through the cell monolayer [3, 5]. As the wave-like propagation of an ERK activity passes through, the direction of collective migration is guided in the direction opposite to that of the ERK wave [4, 5, 8]. This rectification effect would be important for detecting and moving toward a wound to fill the gap in the cell population.

How can the propagation of signaling activity across cell populations, such as the ERK activation waves, affect the collective migration of cells? A physical process that achieves a finite net motion is needed when the signal increases and decreases in one cycle as its wave passes. This requirement is because a spatially symmetric wave does not result in the net motion of cells as the forces generated by the wave are equal in magnitude but opposite in sign. One possible way to address this question is to consider the broken time-reversal symmetry that results from the multiplication of two physical processes [9–11]: if the forces driving cell migration involve more than two processes, time-reversal symmetry can be broken, resulting in net motion, even at force-balance condition [12–16]. However, the existence of these multiplicative effects in collective migration remains unclear. Determining the relationship between directed motion and a traveling signal wave is an important challenge.

* maeda@cheme.kyoto-u.ac.jp

Cell biophysics has contributed greatly to revealing the mechanical model for collective dynamics in a cell monolayer [17–20]. Although individual cells move randomly in the low-density condition, when their density increases, the polarity axis of the cells is oriented by adhesion with neighboring cells, resulting in aligned directions of movement and emergent collective migration. Thus, there is growing interest in elucidating the physical principles of complex tissue formation by characterizing the collective dynamics of cell populations [21, 22]. Numerical models of epithelial collective migration have shown that the orientation dynamics that align polarity and local cell density changes are coupled to produce spatiotemporally ordered structures [23–26]. In the context of wound healing, collective migration guided by ERK signal waves is closely related to the self-repair of epithelial structure, and elucidating the complex processes of epithelial tissue from the perspective of mechanics of collective migration directed by the wave of chemical signaling is important.

In this study, we investigate the mechanics of collective migration along a traveling wave of ERK MAP kinase. We show that by considering the propagation of ERK activation, which regulates both local cell contraction and the cell orientation field in a cell monolayer, directed collective migration can occur in the direction opposite to the ERK wave. Through experimental investigation, we explain key aspects of directed collective migration, such as the non-monotonic increase in migration speed with respect to the activation level and the speed of the ERK wave. Our results indicate that the traveling wave rectifies the direction of collective migration due to a mechanical effect: the interplay of signal-dependent contraction and anisotropic friction.

II. THEORETICAL MODEL OF COLLECTIVE MIGRATION UNDER SIGNALING WAVE

To study how signaling waves control collective migration, we used continuum mechanics. The cell population regulated by intracellular protein signaling can be described as a continuum of two-dimensional coordinates $\mathbf{x} = (x, y)$ (Fig. 1(a)). This theoretical model aims to demonstrate the mechanism controlling collective migration (forward net motion) along a wave of protein signals as it travels through a cell monolayer. Although collective migration is regulated by complex signaling pathways in real cells, it is simplified here to assume that the cell population is activated with a high ERK signal level as it receives ERK kinase signal but this active state gradually decays and returns to the basal state with a low ERK signal level (Fig. 1(b)). The basal level of the protein signal is given by E_0 and takes the same constant value at infinity regardless of the direction. The ERK signal intensity is defined by $\Delta E(\mathbf{x}, t) = E(\mathbf{x}, t) - E_0$, and we assume that the ERK signal is spread by the point source propagating at a constant velocity $\mathbf{u}_l = (u_l, 0)$.

We consider the point source of the ERK signal to have a Gaussian form $\Delta E_0 \exp[-(\mathbf{x} - \mathbf{u}_l t)^2/2a^2]$ with the width of a . The peak size of the ERK signal is ΔE_0 , and in the following analysis, we assume that ERK signal changes follow this distribution function $\Delta E(\mathbf{x}, t)$ in two-dimensional space [27]. Collective migration is driven by internal forces while maintaining force-free conditions [28–33]. The cell population adheres to the substrate and balances the contractile stresses generated by the cells and frictional stress. We considered that both the contractile force and frictional stresses depend on the magnitude of signal activation. The force balance is described as follows:

$$\rho \frac{\partial \mathbf{u}}{\partial t} = -\zeta \mathbf{u} + \nabla \cdot \boldsymbol{\sigma} \quad (1)$$

where $\rho = \rho(\mathbf{x}, t)$ denotes the local cell density, $\mathbf{u}(\mathbf{x}) = (u_x(\mathbf{x}), u_y(\mathbf{x}))$ denotes the velocity field of the cell population, and ζ denotes the frictional coefficient matrix for cell migration per unit area. Cells adhere to each other via cell-cell adhesion junctions, where $\boldsymbol{\sigma}$ represents the internal stress [34, 35]. For an epithelial cell monolayer typically moving at low velocity, the inertia term is negligible, and Eq. (1) is rewritten as

$$\nabla \cdot \boldsymbol{\sigma} = \zeta \mathbf{u}. \quad (2)$$

We defined the internal stress as

$$\boldsymbol{\sigma} = -\Pi \mathbf{I} + kc \mathbf{I} \quad (3)$$

where \mathbf{I} denotes the identity matrix, the first term denotes the density-dependent passive stress caused by the pressure Π , and the second term denotes the signal-dependent stress generated by the molecular motor protein (protein concentration c) with a constant k [34]. However, there is no net motion under changes in density ρ when the friction coefficient ζ does not change with signal activation [32, 33]. This is because the net internal stress (i.e., integral of $\nabla \Pi$ over the cell population) must be zero under force-free conditions. The active stress induced by the molecular motors is insufficient to rectify the directionality of motion relative to the traveling signal wave.

The key concept that defines directed net motion is the multiplication of the frictional force and active contractile force regulated by the protein signal (Fig. 1(c)). Past studies have hypothesized an ERK signaling dependence on adhesion with respect to friction [5, 36], but the specific physical process remains unclear. Instead, we assume that the orientation of the MDCK cell population determines the anisotropy of the friction coefficient and that ERK signaling regulates such anisotropic orientation, which allows us to give a more specific model of the signal dependence of the frictional force.

Cells have an orientation within the cell population, which determines the ease of movement and affects the direction of cell migration [37–39]. The orientation of the cell monolayer is expressed by the director $\mathbf{n}(\mathbf{x}) =$

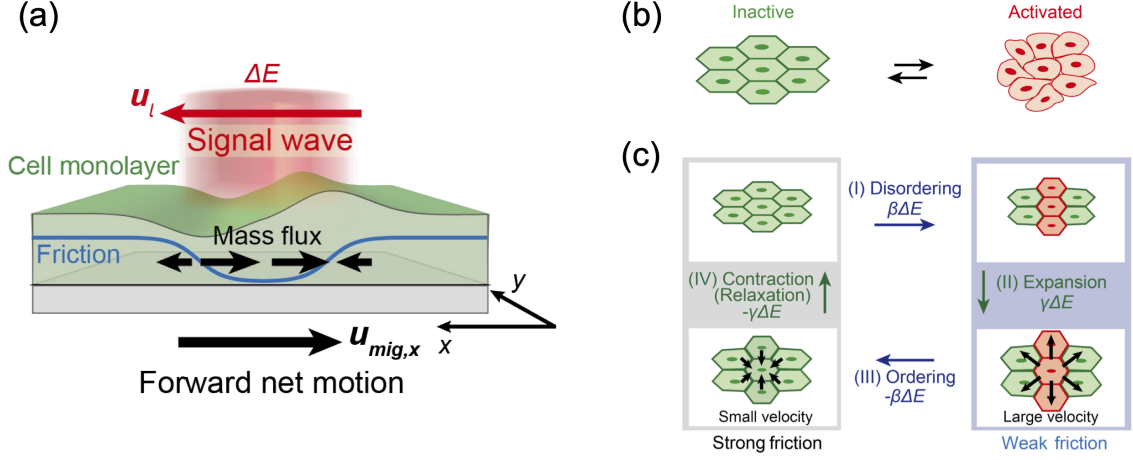


FIG. 1. **Directed collective migration under a traveling signal wave.** (a) Schematic illustration of directed collective migration. The green color indicates a cell monolayer, the height of which represents the change in cell density. (b) Schematic of cell population activated by a signal protein. (c) Schematic illustration of the proposed multiplication of the active contraction and the cellular orientation. The activated signal reduces the anisotropic friction (I: disordering). Signal activation, in turn, causes a cell to be pulled by the surrounding cells (II: expansion). As the signal wave goes through the cell monolayer, the activated cell restores the frictional force (III: ordering) and then it relaxes the pulling force (IV: contraction). Four distinct stages break the time-reversal symmetry in motion.

$(n_x, n_y) = (\cos \theta, \sin \theta)$, with an orientation angle of $\theta(\mathbf{x})$. We assumed that the cell population is oriented along which the signal wave propagates, that is x -direction ($\theta \ll 1$). If this orientation is changed by the signaling activity, the anisotropic mobility may be altered depending on the orientation field and spatially biased by \mathbf{n} .

The tensor of the orientation field is defined as $\mathbf{Q} = S(\mathbf{nn} - \frac{1}{2}\mathbf{I})$ where the scalar order parameter $S = \sqrt{(\cos 2\theta)^2 + (\sin 2\theta)^2}$ is determined from the average θ within the coarse-grained region. S can change in a signal-dependent manner (i.e., $S = S(E)$). The anisotropic friction ζ is given as follows:

$$\begin{aligned} \zeta &= \begin{bmatrix} \zeta_{xx} & \zeta_{xy} \\ \zeta_{yx} & \zeta_{yy} \end{bmatrix} = \zeta_0(\mathbf{I} - \epsilon\mathbf{Q}) \\ &= \zeta_0 \begin{bmatrix} 1 - (\epsilon S/2) \cos 2\theta & (\epsilon S/2) \sin 2\theta \\ (\epsilon S/2) \sin 2\theta & 1 + (\epsilon S/2) \cos 2\theta \end{bmatrix} \end{aligned} \quad (4)$$

where ϵ is the scalar friction parameter representing orientational anisotropy [38]. Negative (or positive) ϵ means that the coefficient of friction for cell migration perpendicular to the orientation angle increases (or decreases). Eq. (4) then gives the viscous resistance force as follows:

$$\zeta \mathbf{u} = \begin{bmatrix} \zeta_{xx}u_x + \zeta_{xy}u_y \\ \zeta_{yx}u_x + \zeta_{yy}u_y \end{bmatrix} \quad (5)$$

We consider a situation in which the cell population migrates in x -axis direction along which the ERK wave propagates. By substituting Eqs. (3) and (5) into Eq. (2), the force-balance relation becomes

$$\zeta_{xx}u_x + \zeta_{xy}u_y = \frac{\partial}{\partial x}(-\Pi + kc), \quad (6)$$

and

$$\zeta_{xy}u_x + \zeta_{yy}u_y = \frac{\partial}{\partial y}(-\Pi + kc), \quad (7)$$

where we use $\zeta_{xy} = \zeta_{yx}$. Eqs. (6) and (7) lead

$$\frac{\partial}{\partial y}(\zeta_{xx}u_x + \zeta_{xy}u_y) - \frac{\partial}{\partial x}(\zeta_{yx}u_x + \zeta_{yy}u_y) = 0. \quad (8)$$

Next, we analyze the mass conservation with a continuum equation. Given that the signal continues to activate the cell body until the wave passes, contractile stress is induced and becomes stronger at the rear of the wave [40, 41]. The resultant gradient of the contractile stress changes the local cell density ρ , which follows the continuity equation

$$\frac{\partial \rho}{\partial t} + \nabla \cdot (\rho \mathbf{u}) = 0. \quad (9)$$

The characteristic time for cell motility is typically estimated as the time required for a cell to traverse a distance approximately equal to its size at a velocity of 15 - 20 $\mu\text{m h}^{-1}$, roughly 1 h. Given that cell division of typical epithelial cells occurs approximately once every 12 h, we consider these time scales to be significantly different. Therefore, we assume that the impact of cell division is negligible.

To find $\mathbf{u}(\mathbf{x})$ that satisfies Eqs. (8) and (9), we use the moving frame coordinate ($\mathbf{x}' = \mathbf{x} - \mathbf{u}_l t$, $\frac{\partial}{\partial t} = -u_l \frac{\partial}{\partial x}$), where the protein signal travels at a constant velocity $\mathbf{u}_l = (u_l, 0)$, and note that u_x , u_y , and ρ have solutions

that depend only on (x', y) . This coordinate transformation rewrites Eqs. (8) and (9) as

$$\frac{\partial}{\partial y}(\zeta_{xx}u_x + \zeta_{xy}u_y) - \frac{\partial}{\partial x'}(\zeta_{yx}u_x + \zeta_{yy}u_y) = 0, \quad (10)$$

and

$$-u_l \frac{\partial \rho}{\partial x'} + \frac{\partial}{\partial x'}(\rho u_x) + \frac{\partial}{\partial y}(\rho u_y) = 0. \quad (11)$$

To solve these equations for perturbations of ERK signal change, we expand the velocity of motion u_i ($i = x, y$) with peak size of the ERK signal ΔE_0 ,

$$u_i = u_{i1} + u_{i2} + \dots \quad (12)$$

where 1 and 2 represent the 1st order and 2nd order of perturbation ΔE_0 , respectively. The cell population does not move without the ERK signal, i.e., $u_{i0} = 0$. We also expand ζ and ρ with ΔE_0 and consider up to the first order written by

$$\begin{aligned} \zeta_{xx} &= \zeta_{xx0} + \zeta_{xx1} + \dots \\ &= \zeta_{xx0}(1 + \beta \Delta E) + \dots \end{aligned} \quad (13)$$

$$\begin{aligned} \zeta_{yy} &= \zeta_{yy0} + \zeta_{yy1} + \dots \\ &= \zeta_{xx0}(1 - \beta \Delta E) + \dots \end{aligned} \quad (14)$$

$$\begin{aligned} \zeta_{xy} &= \zeta_{xy0} + \zeta_{xy1} + \dots \\ &= \zeta_{xy0} + \zeta_{xx0} \beta' \Delta E + \dots \end{aligned} \quad (15)$$

$$\begin{aligned} \rho &= \rho_0 + \rho_1 + \dots \\ &= \rho_0(1 - \gamma a^2 \nabla^2(\Delta E)) + \dots \end{aligned} \quad (16)$$

where $\beta = \frac{1}{\zeta_{xx}} \frac{\partial \zeta_{xx}}{\partial E}$, $\beta' = \frac{1}{\zeta_{xx}} \frac{\partial \zeta_{xy}}{\partial E}$, $\gamma = \frac{\partial \ln \rho}{\partial E}$, and a is the width of the ERK signal distribution. We also assume that S is a minute parameter as small as ΔE . In the density expansion presented in Eq. (16), we assumed the simplest terms that satisfy the mass conservation law and spatial symmetry for any ΔE . The validity of β parameter will be verified in the experiment by the fact that cells tend to move in the oriented direction shown later in Fig. 2. We can write down the expression consisting of the first order terms of ΔE_0 in Eq. (10), by considering $u_{x0} = u_{y0} = 0$,

$$\frac{\partial}{\partial y}(\zeta_{xx0}u_{x1} + \zeta_{xy0}u_{y1}) - \frac{\partial}{\partial x'}(\zeta_{xy0}u_{x1} + \zeta_{yy0}u_{y1}) = 0. \quad (17)$$

Because ζ_{xy0} is $O(S)$ but $\zeta_{xx0} = \zeta_{yy0} = \zeta_0$ are $O(1)$, $\zeta_{xy0}u_{y1}$ and $\zeta_{xy0}u_{x1}$ can be negligible. By this approximation, Eq. (17) becomes vortex-free relation $\frac{\partial u_{x1}}{\partial y} - \frac{\partial u_{y1}}{\partial x'} = 0$.

Furthermore, we find the relation that is also valid for the density ρ in the first order of ΔE_0 from Eq. (11).

$$-u_l \frac{\partial \rho_1}{\partial x'} + \rho_0 \frac{\partial u_{x1}}{\partial x'} + \rho_0 \frac{\partial u_{y1}}{\partial y} = 0. \quad (18)$$

Using $\rho_1 = -\rho_0 \gamma a^2 \nabla^2 \Delta E$, Eq. (18) is rewritten by

$$-u_l \gamma a^2 \frac{\partial}{\partial x'} \nabla^2 \Delta E = \frac{\partial u_{x1}}{\partial x'} + \frac{\partial u_{y1}}{\partial y}. \quad (19)$$

The solution of u_{x1} that satisfies Eqs. (17) and (19) is

$$u_{x1} = -u_l \gamma a^2 \frac{\partial^2 \Delta E}{\partial x'^2}. \quad (20)$$

If $\Delta E = \partial \Delta E / \partial x' = 0$ at infinity ($x, y \rightarrow \infty$), the spatial average of $\partial^2 \Delta E / \partial x'^2$ is also zero. We thus find that spatial average of u_{x1} is also zero, meaning that net motion is not realized within the first order. Therefore, to explain collective motion under signal waves, we need to solve for u_2 .

We write the second-order term of the ERK signal change in Eq. (10). Since ζ_{xy0} is small in $O(S)$, we can ignore the terms that include ζ_{xy0} as coefficient:

$$\frac{\partial}{\partial y}(\zeta_{xx1}u_{x1} + \zeta_{xx0}u_{x2} + \zeta_{xy1}u_{y1}) - \frac{\partial}{\partial x'}(\zeta_{xy1}u_{x1} + \zeta_{yy1}u_{y1}) = 0. \quad (21)$$

We consider that there is no net motion in the direction perpendicular to the ERK wave (see detailed calculation in [27]). Eqs. (13)-(16) give $\zeta_{xx1}/\zeta_{xx0} = \beta \Delta E$, $\zeta_{yy1}/\zeta_{xx0} = -\beta \Delta E$, and $\zeta_{xy1}/\zeta_{xx0} = \beta' \Delta E$. By substituting these coefficient relationships into Eq. (21) and integrating in the y direction, u_{x2} is determined by

$$\begin{aligned} u_{x2} &= -u_{x1} \beta \Delta E - u_{y1} \beta' \Delta E \\ &\quad - \beta \frac{\partial}{\partial x'} \int_{-\infty}^y dy u_{y1} \Delta E + \beta' \frac{\partial}{\partial x'} \int_{-\infty}^y dy u_{x1} \Delta E. \end{aligned} \quad (22)$$

We are interested in the spatial average in the x direction, $\langle u_{x2} \rangle_x$. From the symmetric distribution of E , u_{x1} and ΔE are even functions in x and y while u_{y1} is an odd function. Considering that ΔE and u_{y1} are zero at the far end, only the first term on the right side of eq.(22) contributes as

$$\frac{1}{\sqrt{\pi}a} \int_{-\infty}^{\infty} dx' u_{x2} \equiv \langle u_{x2} \rangle_{x'} = -\langle u_{x1} \beta \Delta E \rangle \quad (23)$$

(see detailed calculation in [27]). We recall that u_{x1} is derived as Eq. (20) from the continuum equation. By performing a partial integral, we obtain

$$\begin{aligned} \langle u_{x2} \rangle_{x'} &= u_l \beta \gamma \frac{a}{\sqrt{\pi}} \int_{-\infty}^{\infty} dx' \Delta E \frac{\partial^2 \Delta E}{\partial x'^2} \\ &= -u_l \beta \gamma a^2 \left\langle \left(\frac{\partial \Delta E}{\partial x'} \right)^2 \right\rangle_{x'}, \end{aligned} \quad (24)$$

which indicates that $\langle u_{x2} \rangle_x \neq 0$ whenever ERK signal distribution has a point $\partial \Delta E / \partial x' \neq 0$. Finally, by converting the coordinates from the moving frame to the experimental frame ($x' \rightarrow x$ and $\partial / \partial x' \rightarrow \partial / \partial x$), we then perform the calculation of the Gaussian shape of ΔE at $y = 0$ on the propagation path of the ERK wave. Migration velocity $\mathbf{u}_{mig} = (\langle u_{x2} \rangle_x, 0)$ at $y = 0$ is

$$\mathbf{u}_{mig} = -\mathbf{u}_l \frac{\beta \gamma}{2} (\Delta E_0)^2. \quad (25)$$

This form of \mathbf{u}_{mig} indicates nonzero net motion under the propagating ERK wave (Fig. 1(a) and (c)). $\beta\gamma > 0$ indicates that the cell population migrates in the opposite direction of the approaching signal wave and persistently drives the net motion in one direction. Note that β appears in Eq. (25) reflects the response of the friction coefficient to the ERK change (Eqs. (13)-(15)), while γ in Eq. (25) comes from the response of the ERK-dependent cell density (Eq. (16)). Therefore, these two parameters have different physical origins, and their product determines the speed of the ERK wave-driven collective migration.

III. ERK SIGNALING IN MDCK CELL MONOLAYER AS AN EXPERIMENTAL MODEL

We experimentally verified the theoretical model using monolayer-forming epithelial cells. We used Madin-Darby canine kidney (MDCK) cells because they exhibit collective migration coupled to intracellular signaling activation. In a monolayer of MDCK cells, the activity of ERK MAP signaling (ERK signaling) propagates like a traveling wave and drives collective migration in the opposite direction of the signal wave [2, 5, 42]. During collective migration, ERK signaling regulates contractility through the myosin molecular motor. ERK propagates through the cell monolayer as a traveling wave, exhibiting rectified migration. The presence of cells with high ERK activity in a cell population can also induce spatial changes in the contractile force gradient and orientation order between cells. Consequently, we considered an ERK-regulated MDCK cell monolayer to be an appropriate experimental system for our theoretical model.

The MDCK cells used in the experiment were optogenetically controlled through the ERK pathway using light-induced dimerization (LID) of CRY2-CIBN [3, 5] (Fig. 2(a)) with 488 nm blue LED laser. The phosphorylation activity of ERK MAP kinase increased in response to light intensity, during which ERK-mCherry protein was translocated to the nucleus (Fig. 2(b)). This tool allowed for manipulating the ERK activity at the single-cell level in a light-responsive manner. Because the ratio of the amount of ERK-mCherry partitioned between the cytoplasm and nucleus is proportional to ERK activity in this setup (Fig. S1 [27]), the level of activity was quantitatively assessed by measuring the nuclear translocation of ERK-mCherry proteins (Fig. 2(c)). The detailed calculation method of ERK activity is provided in the Supplemental text [27].

We tested whether light could regulate ERK signaling activity and thereby induce changes in MDCK cell density and orientation within the monolayer. To perform this analysis, we included a light-unresponsive cell population to create differences in signal intensity between cells. We made a mosaic cell population by mixing the optogenetic MDCK cells with normal cells at a 1:9 ratio. This heterogeneous cell population was then exposed to

blue light, which induced ERK signaling only in light-responsive cells. After applying optogenetic activation for 30 min, we tested whether the activated cells exhibited an increase in the cell area. The ratio of changes in cell area is a non-dimensional parameter defined as $(A_1 - A_0)/A_0$, where A_0 and A_1 are the cell area before and after optogenetic ERK activation, respectively. The activated cells showed a clear increase in the change of cell area in proportion to ERK activity (Fig. 2(d)). However, significant change in cell area was not observed in a single isolated cell (Fig. 2(e)). These results suggest that the cell area has expanded due to forces generated by the activated cells pulling on the inactive cell. We also found with the aid of traction force microscopy that intracellular contractility decreased in MDCK cells with elevated ERK activity (Fig. S3) [27, 43], indicating that cells with increased ERK activity have decreased contractility. The surrounding cells maintain their contractility, resulting in an enlarged area due to the pulling from surrounding cells. Thus, because the cell spreading area is increased by ERK activity, local activation of ERK signaling results in reduced cell density, $\gamma < 0$.

We also investigated whether the isotropy of the cell orientation is influenced by ERK activation by inducing the light stimulation to optogenetic MDCK and analyzing the cell orientation order. The orientation order parameter before light exposure was set to S_0 ; after optogenetically upregulating ERK activity for 30 minutes, the difference in the orientation order $\Delta S = S - S_0$ was analyzed at different levels of ERK activity. As ERK activity increased, the rate of change in the orientation order decreased (Fig. 2(f)), indicating that the orientation of the cell population became more random due to ERK activation. A mix of optogenetic MDCK and normal MDCK cells was only used for the experiments shown in Fig. 2(d)-(f).

Previous studies on MDCK cell populations reported that the velocity tends to increase when cells move parallel to the orientation angle [37, 44]. In the present study, on the contrary, we introduced the relationship between the changes in orientation order and friction, as seen in Eq. (4). The decrease in friction in the direction of alignment corresponds to a negative friction parameter, $\epsilon < 0$ (the opposite is observed in neural progenitor cells, where $\epsilon > 0$ [38]). According to $\beta \sim -\epsilon \frac{dS}{dE}$, the change in the friction coefficient in our experiment ($\epsilon < 0$, $\frac{dS}{dE} < 0$) was $\beta < 0$.

IV. COLLECTIVE MIGRATION UNDER A SYNTHETIC ERK WAVE

Experiments on the optogenetic control of ERK suggest that MDCK cells respond to an increase in ERK signaling with a friction change of $\beta < 0$ and density change of $\gamma < 0$. Eq. (25) indicates that $\beta\gamma > 0$, suggesting that the motion is in the opposite direction to the ERK signal wave. To test this theory, we designed

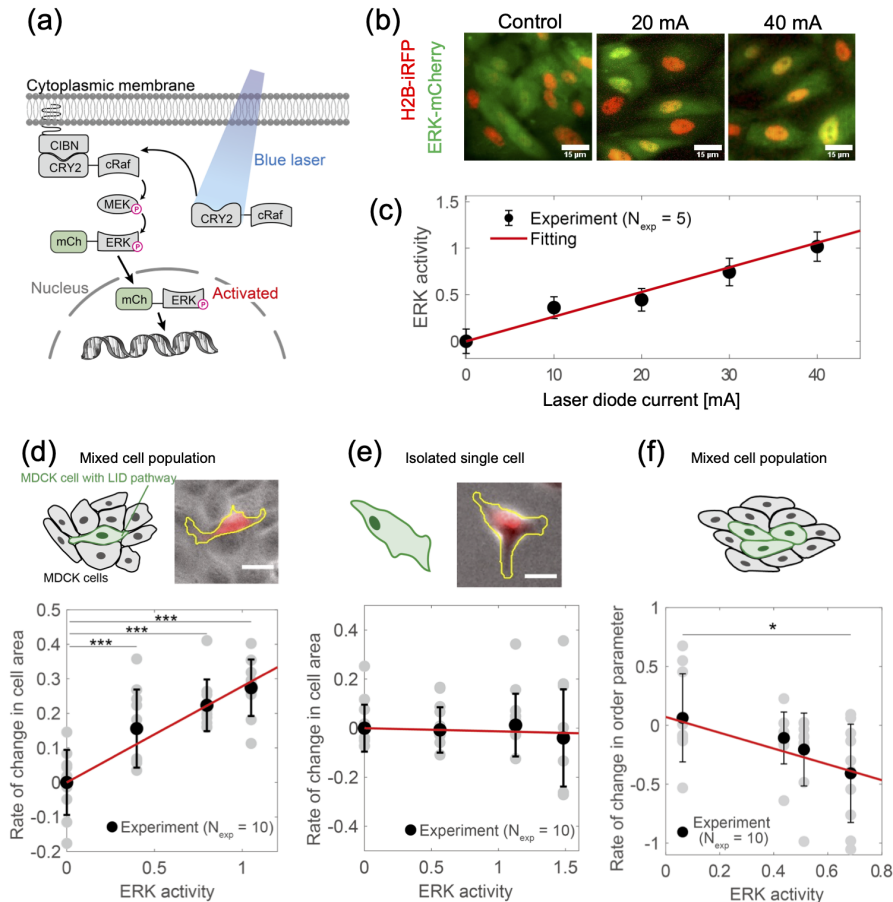


FIG. 2. Controlling epithelial cells with optogenetic ERK signal activation. (a) Optogenetic control of ERK activity through light-induced dimerization. (b) Fluorescent imaging analysis for quantifying ERK activity, ΔE . In the absence of light, ERK-mCherry is found in the cytoplasm. ERK signaling induces the nuclear translocation of ERK-mCherry (denoted by H2B-iRFP in red) through transduction. The extent of nuclear migration is directly proportional to the degree of substrate phosphorylation by the ERK MAP kinase. ERK activity can be regulated quantitatively by adjusting light intensity. Scale bars: 15 μm . (c) Linear calibration plot of ERK activity for optogenetic light intensity. The experimental data is represented by black dots. The red line represents the linear curve with the slope $g=0.022$ with 95% confidential interval (CI) of 0.011 to 0.029. The numbers of technical replicates is $n = 1$ and the number of independent experiments is $N_{exp} = 5$. (d) Changes in the area of ERK-activated cells in the mixed cell population (bottom). The red line is the fitting linear curve with the slope $g=0.25$ (95% CI is 0.18 to 0.33). Schematic illustration of light-inducible dimerization (LID) pathway in the mixed cell population (top). A cell with LID pathways was outlined with the yellow line, and the nucleus is shown in red. (e) Changes in cell area in isolated single cells (bottom). The red line is the fitting linear curve with the slope $g=-0.01$ (95% CI is -0.11 to 0.09). Schematic of single cells activated through the LID pathway (top). (f) Changes in orientation order in ERK-activated cells in the mixed cell population (bottom). The red line is the fitting linear curve with the slope $g=-0.44$ (95% CI is -0.71 to -0.17). Data were analyzed using the Mann-Whitney U-test, *** $p < 0.001$, * $p < 0.05$. In (d)-(f), the number of technical replicates is $n = 2$ for (d) and (e) or $n = 3$ for (f), and the number of independent experiments is $N_{exp} = 10$. The black circle indicates the mean value and the error bar is the SD.

a synthetic ERK wave mimicking a natural signal wave through the unidirectional sweeping of a focused laser light (Fig. 3(a)). MDCK cell population was confined in 500 μm wide channel-shaped region. This confinement size is only slightly larger than the velocity correlation length of the MDCK cell monolayer (that is approximately 300 μm [45]), and is large enough to achieve a one-dimensional system without strong effects of constraints. The area covered by the laser light used for optogenetics

is $\sim 100 \mu\text{m}$ in diameter, and spatial differences in ERK activity are produced with and without light stimulation. Therefore, the situation shown in Figure 2(d), where cells with high ERK activity are surrounded by cells with low ERK activity at the basal level, is realized by this optogenetic manipulation.

The synthetic ERK wave travels at a constant speed $u_l = 2.0 \mu\text{m}/\text{min}$, whereas ΔE is regulated by adjusting the laser intensity. The velocity of cell migration was al-

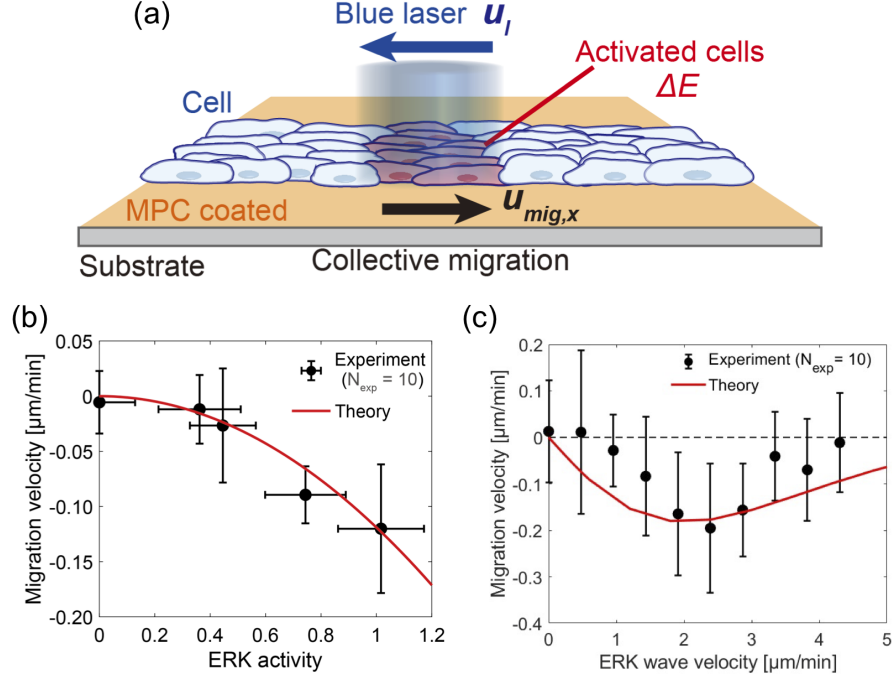


FIG. 3. **Directed collective migration of MDCK cells guided by a synthetic signal wave.** (a) Collective migration by a sweeping synthetic ERK wave. The cell monolayer with the LID pathway was patterned into a channel-shape of width $500\ \mu\text{m}$. A spot of blue light was moved along the cell monolayer at a velocity of u_l . (b) Squared dependence of the migration velocity on the magnitude of the synthetic ERK wave. The theoretical curve was drawn by fitting with Eq. (25) with $\beta\gamma = 0.14$ (95% CI is 0.00 to 0.28). The number of technical replicates is $n = 2$, and the number of independent experiments is $N_{exp} = 10$. The error bars in horizontal and vertical axes indicate the SD. (c) Wave-speed dependent collective migration. The maximum velocity of the migration occurred at an intermediate ERK wave speed (black circles). The theoretical curve of Eq. (26), which also includes the calculation according to Eq. (27), was fitted with $\beta\gamma = 0.12$ (95% CI is 0.00 to 0.25) and fixed parameters $\tau_d = 40\ \text{min}$, $\lambda = 450\ \mu\text{m}$, and $\tau_E = 15\ \text{min}$ [3] (solid red lines in (b) and (c)). The number of technical replicates is $n = 2$, and the number of independent experiments is $N_{exp} = 10$. The error bars indicate the SD.

ways negative, indicating that the cell population with increased ERK activity moved in the direction opposite to that of the ERK wave (Fig. 3(b)). Moreover, as expressed in Eq. (25), the collective migration speed $|\mathbf{u}_{mig}|$ is proportional to the square of ERK activity, $(\Delta E)^2$. In the experiment, the migration velocity exhibited a quadratic increase with ΔE (Fig. 3(b)). Our theoretical model is thus consistent with experimental observations; in particular, the quadratic increase in migration speed implies that the two ERK-dependent processes of density and friction are involved in rectifying collective migration under the traveling signal wave.

We measured the dependence on the ERK wave velocity and found that the maximum migration velocity $u_{mig} = -0.2\ \mu\text{m}/\text{min}$ was reached at a wave velocity of $u_l = 2.3\ \mu\text{m}/\text{min}$ (Fig. 3(c)). Such a wave velocity in directed collective migration has also been reported in previous studies [5, 11, 42]; however, the mechanical mechanisms remain unclear. Accordingly, we considered viscoelastic deformation and restoration in cell migration. The extended deformation coefficient is $\Gamma_{\tau_d} = \gamma \left[1 - \exp\left(-\frac{\lambda}{u_l \tau_d}\right) \right]$, where τ_d is the characteristic

time of mechanical restoration ($\tau_d \approx 40\ \text{min}$ [46]) and λ is the wavelength of the ERK wave ($\lambda = 450\ \mu\text{m}$) (see detailed calculation in [27]). By considering the relaxation time in the density change in Γ_{τ_d} [47], the migration velocity \mathbf{u}_{mig} can be extended to the general form

$$\mathbf{u}_{mig} = -\mathbf{u}_l \frac{\beta \Gamma_{\tau_d}}{2} (\Delta E_0)^2. \quad (26)$$

Γ_{τ_d} affects the migration speed according to the relationship between the relaxation time of the density (τ_d) and the propagation time of the wave ($\frac{\lambda}{u_l}$). For slowly propagating ERK waves ($u_l/\lambda \ll 1/\tau_d$), the migration velocity $u_{mig} \propto u_l(1 - \exp[-\lambda/(u_l \tau_d)]) \sim u_l$ and thus migration speed linearly increase with ERK wave speed. Hence, the relaxation process can explain the gradual increase in u_{mig} at low wave speeds.

In contrast, for rapidly propagating ERK waves ($u_l/\lambda \gg 1/\tau_d$), the migration velocity plateaus at $u_{mig} \propto u_l(1 - \exp[-\lambda/(u_l \tau_d)]) \sim \lambda/\tau_d$. This means that the migration velocity does not decrease at large u_l , and we need to consider another relaxation process to explain the non-monotonic increase of the migration velocity. To address this point, we also consider the decay of signaling

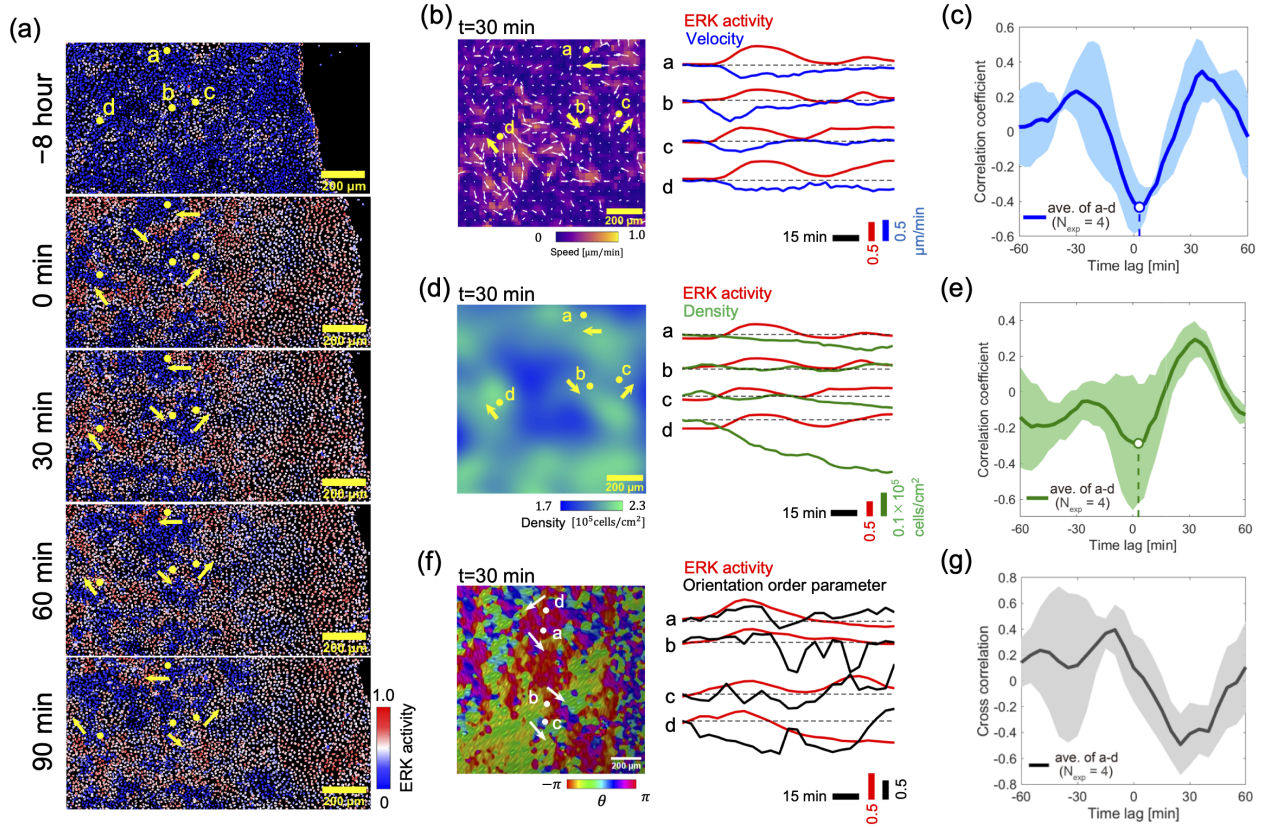


FIG. 4. **ERK wave-driven collective migration in the wound healing process of MDCK cells.** (a) Spatiotemporal alterations in ERK activity within the wound-healing MDCK cell population, as measured using a FRET probe, with red indicating heightened levels of ERK activation. The yellow dots indicate the positions where the time course of ERK activity, migration velocity, orientation order, and cell density are plotted as representative data in Fig. 4(b), (d), and (f), respectively. Alphabetical letters are used to distinguish between these points. The yellow arrows indicate the direction of ERK wave propagation, determined by the ERK activity measured using a FRET probe. The time $t = 0$ was defined as 8 h after the start of the wound healing assay. (b) Time course of cell migration speed and ERK activity within the cell monolayer. The reference value at $t = 0$ is indicated by the dotted line was used to evaluate the degree of change in migration velocity (density in (d) and orientation order in (f)) from the basal level. (c) Cross-correlation function between ERK activity and cell migration. A negative simultaneous correlation indicates that the collective migration opposing the ERK wave dominates wound healing propagation. (d) Time course of ERK activity and cell density. (e) Cross-correlation function between ERK activity and fluctuations in cell density. A negative correlation at a time lag of $\Delta t = 0$ indicates that an increase in ERK activity is correlated with a decrease in cell number density. (f) Cell orientation dynamics. The orientation angle of individual cells within the cell monolayer is displayed through a color code. Changes in the orientation order parameter S are plotted with ERK activity over time. (g) Cross-correlation function between orientation order and ERK activity. A negative correlation value of $\Delta t = 30$ min indicates that an increase in ERK activity is associated with a decrease in orientation order. In Figs. 4(b) - (g), four data points ($N_{exp} = 4$) were collected in the measurement of the wound-healing cell population, and the number of technical replicates is $n = 1$ for these measurements. The image data used for orientation analysis in Fig. 4(f) is different from those used for Figs. 4(b) and 4(d).

activity with increasing u_l . The relaxation dynamics of ERK signaling are given by

$$\frac{d\Delta E}{dt} = -\frac{\Delta E}{\tau_E} + I_s, \quad (27)$$

where $I_s(\mathbf{x}, t) = I_0 \exp(-(\mathbf{x} - \mathbf{u}_l t)^2 / 2a^2)$ is the point source of the signal wave and τ_E is the relaxation time of the activated signal [5, 27]. The duration of signal activation is defined as the time scale $T \approx b/u_l$, with a

typical cell size of $b = 20 \mu\text{m}$. If the activation time T is sufficiently longer than the ERK signal relaxation time τ_E ($T \gg \tau_E$), ΔE is fully activated by the saturation level, and no change appears in \mathbf{u}_{mig} for the slowly propagating ERK wave. However, if the activation time is shorter than the relaxation time ($T \ll \tau_E$) under fast-moving waves, ΔE decreases, in turn damping the associated changes in contractile stress and reduction in friction over time. Because of such a reduction of ΔE

at large u_l , the migration velocity u_{mig} decreases at fast propagating ERK wave (Fig. 3(c)).

Therefore, the interplay between density relaxation and signal activation may determine the ERK wave speed of the fastest motion. Our model predicted such wave velocity as $u_l = 2 \sim 3 \mu\text{m}/\text{min}$, which is comparable to the experimental value of $2.3 \mu\text{m}/\text{min}$ (Fig. 3(c)).

V. WOUND HEALING OF EPITHELIAL CELL MONOLAYER

The proposed model of wave-directed collective migration inspires an experimental investigation of the interplay between naturally occurring signaling waves and the mechanics of the epithelial cell monolayer during wound healing (Fig. 4(a) and Supplemental Movie 1). In wound healing experiments, MDCK cell populations were cultured in internal compartments of removable chambers to obtain monolayers, and the compartment walls were removed when they reached a confluency that indicated collective migration from the leading edge [5]. This allowed the *in vitro* wounded areas to spread to those where cells were not present, defined as an injured region. We obtained time-lapse images for quantitatively measuring ERK signaling. The level of ERK activation was reported with a FRET sensor of ERK phosphorylation, which was expressed in the cell nucleus, and both cell motility and ERK activity levels were simultaneously measured by time-lapse fluorescence microscopy (see supplemental materials [27]). ERK activity remained high in the leading edge of the cell population during wound healing, and ERK wave generation occurred far away. Therefore, the analysis of ERK waves was targeted to the region $500 \mu\text{m}$ away from the wound edge. Upon the removal of the compartment walls from the cell monolayer, directed collective cell migration is initiated, leading to wound closure. The initiation of collective migration applies mechanical stimuli to the leading cell layer, which activates ERK signaling. The FRET sensor for ERK activation showed that the highly active region (red cells) was localized near the wound site, indicating that ERK signaling propagated from the leading edge of the wounded cell population (Fig. 4(a)). It has been shown that cells collectively migrate in the direction opposite to the propagation of the ERK wave and then fill the existing wound starting from the leading edge [4, 5, 42]. By measuring the intensity of ERK signaling and cell migration relative to the direction of ERK wave propagation, we observed that the speed of cell motility increased as the intensity of the signal decreased (Fig. 4(b)), indicating a negative correlation between motility speed and changes in ERK signaling (Fig. 4(c)). We examined changes in cell density associated with ERK activity during wound healing. Cell density was evaluated based on the number density of cells in a square with $101 \mu\text{m}$ side length. Although the theoretical model considers the cell's mass density, it is represented using the ratio of the area occupied by

cells in the experiment. We found that local cell density decreased with increased signaling (Fig. 4(d) and (e)), consistent with previous findings [5, 40].

We analyzed the orientational dynamics of MDCK cells induced by ERK signaling. The orientation angle $\theta(\mathbf{x})$ in the cell monolayer was calculated from bright-field images (Fig. 4(f), left)[27]. The orientation field was then used to calculate the scalar order parameter $S(\mathbf{x}) = \sqrt{\langle \cos 2\theta \rangle_{ROI}^2 + \langle \sin 2\theta \rangle_{ROI}^2}$ by averaging over the region of interest (ROI). We analyzed the signal-dependent change in $S(\mathbf{x})$ and found that this order parameter decreased as ERK activity increased (Fig. 4(f), right). We also calculated the correlation between ERK signaling and $S(\mathbf{x})$ and observed a negative cross-correlation function with a time delay $\Delta t = 30 \text{ min}$ (Fig. 4(g)), indicating that local orientation becomes less organized as ERK activity increases. For a typical ERK wave size of $\lambda = 450 \mu\text{m}$ and an ERK wave velocity of $u_l \approx 2.0 \mu\text{m min}^{-1}$, cells are exposed to ERK activity for an activation time $T \approx 220 \text{ min}$ activation. From the time delay $\Delta t \approx 30 \text{ min}$ shown in Fig. 4(g), this duration of ERK activation is significantly longer than the relaxation time of the Q tensor ($\approx 30 \text{ min}$). This indicates that the spatial distribution of the Q tensor becomes stationary upon activation by the ERK wave. Assuming that the local orientation order is related to anisotropic friction, the ERK signal wave may facilitate the reorientation of cells along the direction of wave propagation, making it easier for the cell population to move in that direction.

To extend our theoretical model to wound healing [48–51], we considered a cell monolayer whose leading edge can move in one direction (Fig. 5(a)). We assumed that the ERK signal propagates from the wound site at speed \mathbf{u}_l within the cell monolayer, whereas the leading cells move toward the wound region at the constant speed $\mathbf{u}_w = (u_w, 0)$. This motion of the leading cells induces an outward density flux in the cells, $\mathbf{J}_w = \rho \mathbf{u}_w$ (Fig. 5(b)). The cell population then moves at a velocity of \mathbf{u}_{mig}^{wh} against the protein signal wave generated from the wound. Given that the cell population maintains a continuous cell monolayer, Eq. (9) is rewritten as $\frac{\partial \rho}{\partial t} + \nabla \cdot (\rho \mathbf{u}_{mig}^{wh}) = -\nabla \cdot \mathbf{J}_w$. In the moving frame of a traveling signal wave, the density flux is $-(u_l - u_w) \frac{\partial \rho}{\partial x'} + \frac{\partial \rho}{\partial x'} (\rho u_x) + \frac{\partial}{\partial y} (\rho u_y) = 0$, showing that the effective velocity of the signal wave is $\mathbf{u}_l - \mathbf{u}_w$ in a system at the tip of the signal wave. The migration velocities in Eq. (26) can be given by (see detailed calculation in [27])

$$\mathbf{u}_{mig}^{wh} = -(\mathbf{u}_l - \mathbf{u}_w) \frac{\beta \Gamma_{\tau_d}}{2} (\Delta E_0)^2. \quad (28)$$

Eq. (28) indicates that the migration speed is a multiplicative expression as a product of β and Γ_{τ_d} , with the only difference being that the wave velocity is $\mathbf{u}_l - \mathbf{u}_w$. We compared the theoretical models with wound healing experiments by measuring ERK wave velocity and analyzed the rate of leading-edge spreading. We plotted the migration velocity scaled by the ERK signal

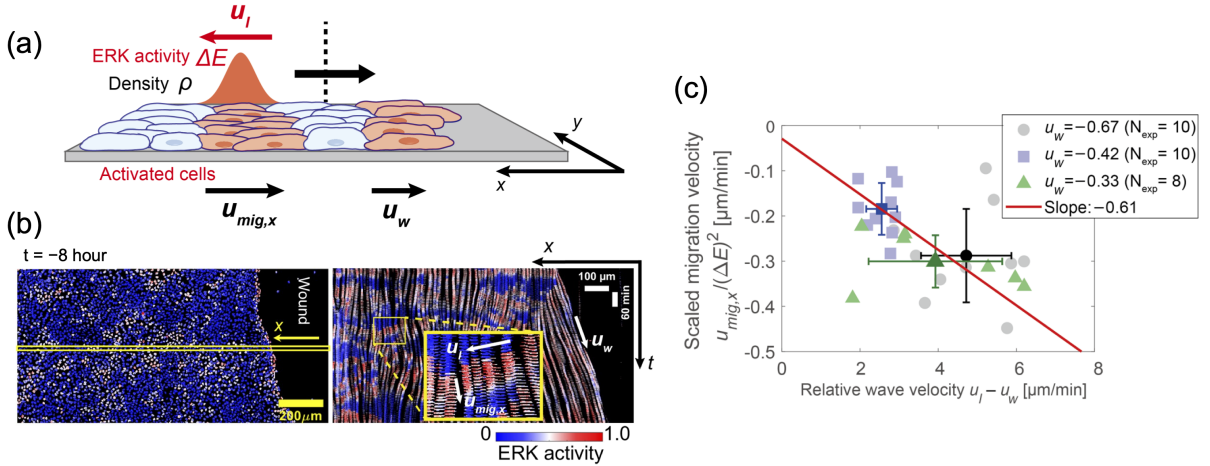


FIG. 5. **Collective migration in a traveling ERK wave during wound healing.** (a) Schematic of collective migration associated with the ERK wave during wound healing. We consider the edge of MDCK cell monolayer move at wound progression u_w . (b) Quantification of the ERK wave speed u_l , migration speed $u_{mig,x}$, and wound progression speed u_w . We measured the speed parameters from the kymograph of MDCK cells undergoing wound healing. In Fig. 4(a), the image at the left shows MDCK cells at $t = -8$ h. Cell nuclei were visualized and detected by the fluorescent probe, with the spatial axis toward the wound region on the horizontal axis and the time axis on the vertical axis. The color of the labeled cell nucleus represents the intensity of ERK activation as indicated in the color bar. (c) Relationship between migration speed and ERK wave speed. Data plotted in different colors represent three independent experiments. The ERK activity ΔE was measured using a FRET probe sensor. ERK activity was normalized against its maximal value. Each data point corresponds to directed migration under one ERK wave. The solid line represents Eq. (28) with $\beta\gamma = 0.11$ (95% CI is 0.02 to 0.23), with fixed parameters $\tau_d = 40$ min and $\lambda = 450$ μm . The number of technical replicates is $n = 3$, and the number of independent experiments is $N_{exp} = 8$ or 10.

level $u_{mig}^{wh}/(\Delta E_0)^2$ for the stretching velocity of the ERK wave $u_l - u_w$ (Fig. 5(c)), and found a linear relationship as proposed by Eq. (28). The slope of the curve was expressed as the product of the coefficients of the ERK-dependent density change β and the friction change γ . Here, $\beta\gamma = 0.11$ was comparable between the wound healing and optogenetic manipulation experiments ($\beta\gamma = 0.12$ in Fig. 3(c)).

VI. DISCUSSION

This study showed that the coordination of changes in cell density and friction as a function of signal activation-induced net collective migration was rectified against a traveling signal wave. Around the trailing end of the signal wave, the friction coefficient decreased and the contractile stress increased. Consequently, the pulling force from the rear end drives forward net motion of the cells. However, at the front end of the wave, cell stretching accentuated the velocity of motion in the direction opposite to the wave. To summarize the mechanism of this collective migration, the driving force results from the multiplicative effect of the active stress and friction changes generated by the ERK signal. The signal-dependent active stress causes a local density change, and density flow is generated by the tug-of-war between neighboring cells. Such density flow is biased by ERK-dependent cell orientation, which generates an anisotropic friction gradient.

Thus, the two ERK-dependent effects work together to drive directed collective migration, and their speed exhibits a quadratic increase ($u_{mig} \propto (\Delta E)^2$) in ERK signal intensity. In our continuum model, two basic equations, the conservation of momentum Eq. (1) and continuity equation Eq. (9), were used to derive the equation of unidirectional collective migration under the ERK signal wave. The unidirectional net motion is induced by the ERK signal-dependent anisotropy of the friction coefficient and density change, which are reduced to β and γ parameters, respectively. The advantage of the continuum model presented in this study is the representation of the dynamics of the collective motion by these important parameters.

Theoretical models proposed in previous studies [52, 53] have elucidated how cell monolayers can establish polarity in cell migration, attributed to the temporal delay in stress response relative to changes in ERK activity. As the feedback mechanism between ERK wave signaling and cellular stress fields, the self-organized ERK waves can be stabilized during wound healing. In contrast, our study introduces the concept of nematic order in cell alignment and orientation-dependent friction coefficients, replacing wave-induced polarization. We assume that ERK-dependent friction reduction mediated by nematic order is crucial in inducing directional symmetry breaking of collective migration. This perspective offers a physical basis for explaining the breaking of the symmetry of directed collective migration, unlike previous

studies. In addition, we consider the continuum equation in a cell monolayer that does not involve cell rearrangement. Therefore, we formulated the relaxation dynamics using viscoelastic relaxation based on the Voigt model [27]. Previous research has reported that when epithelial cells rearrange to overcome column obstacles, they behave like an effective viscous fluid following the Maxwell model [54]. It should be noted, however, that in our wound-healing assay, migrating cells do not experience confinement by obstacles, but rather recover their original cell orientation after complete relaxation from ERK signaling activation, resulting in an elastic response.

Moreover, another theoretical model [5, 36] suggested that ERK activation affects the frictional force of cell motility by assuming a change in magnitude. In Eq. (4), we considered that the signal-dependent mobility is controlled by the orientation dependence, not the magnitude of the friction coefficient. This was confirmed by our measurements of adhesion strength in single cells with increased ERK activity, which showed no ERK dependence on the adhesion magnitude (Fig. S4 of [27] and [55, 56]). This suggests that the critical change in friction is likely associated with the orientation of the cell-cell interactions. However, the magnitude of the friction coefficient may yet depend on ERK activation at the cell-population level. Recent studies have shown that the interplay between contractile stress and epithelial cell polarity [42, 57] is involved in directed collective migration. Thus, the exact mechanisms of signal-dependent orientation changes remain a future challenge [58].

The cell monolayer can control collective migration by regulating the phase difference between two cyclical changes in density and friction while maintaining the force balance. We also found that the existence of the ERK wave speed at which the migration speed is maximal is explained by the interplay of two relaxation dynamics of the cell density change and the decay of the ERK signal. Although we assume that the rate of decay of signaling is faster than that of density change, it is an important question to experimentally test whether the two relaxation times are different enough to explain the ERK-wave speed dependence. A further understanding of the mechanical coordination of contraction and friction, including force-signaling feedback [52], may provide physical insights into the active dynamics organized by a traveling signal wave. Understanding how signal transduction systems regulate directed collective migration and ordered pattern formation, not only in epithelial cells but also in other cell types, such as stem cells [38, 59], will aid in understanding the principles by which cell populations build functional forms while adapting to complex geometric constraints [45, 60, 61]. Such interplay of mechanical force and protein signaling is involved in apoptosis [62] and tissue regeneration [63]; therefore, elucidating the physical mechanisms underlying these mechanical-chemical interactions is an important challenge for future research.

ACKNOWLEDGEMENTS

This work was supported by Grant-in-Aid for Scientific Research on Innovative Areas (JP16H00805, JP17H05234, and 18H05427 to YTM, JP19H05798 to KA), Grant-in-Aid for Transformative Research Areas (A) (JP23H04711 and JP23H04599 to YTM), Grant-in-Aid for Scientific Research (B) (JP20H01872 and JP23H01144 to YTM, JP18H02444 and JP22H02625 to KA), Grant-in-Aid for Young Scientists (JP22K14014 to TF), JST FOREST Grant (JPMJFR2239 to YTM), CREST JST Grant (JPMJCR1654 to KA), AMED-CREST Grant (JP20GM0810002 to SK), NIBB Collaborative Research Program (18-355 to YTM), Research Grant from Nakatani Foundation (to YTM), and Joint Research of ExCELLS (23EXC205 and 24EXC206 to YTM).

APPENDIX

A. Materials and Methods

An epifluorescence microscope (Olympus, IX73) equipped with a CMOS camera (Andor, Zyla) was used for microscopic observation. The nuclei were labeled with H2B-iRFP fluorescent protein to track individual cells, and live fluorescent imaging was taken at 5-minute intervals for 8 h. The cell migration velocity was calculated by dividing the change in the position of the fluorescent protein-labeled cell nucleus by the time interval of 5 min. For the experiment in Fig. 3, to ensure that cell migration occurs along optogenetically induced ERK signal wave, MDCK cells were seeded in a quasi-one-dimensional channel pattern with the width of 500 μm by a micropatterning method previously reported [61].

MDCK cell line was cultured in MEM (ThermoFisher Scientific, 11095-072) supplemented with 10% fetal bovine serum (FBS; Sigma-Aldrich, 172012-500mL), 1x GlutaMax (ThermoFisher Scientific, 35050061), and 1 mM sodium pyruvate (Sigma-Aldrich, S8636-100mL) in a 5.0% CO₂ humidified incubator at 37 °C. We also used optogenetic MDCK cells (MDCK/CRY2-CRaf/CIBN-EGFP-KRasCT/H2B-iRFP/FLAG-MEK1-mCFP/mCherry-ERK2KD) established in Ref.[5](Fig. 2(a)). MDCK cells expressing CRY2-CRaf, CIBN-EGFP-KRasCT, H2B-iRFP, FLAG-MEK1-mCFP, and mCherry-ERK2KD were selected with antibiotics and then maintained in a minimum essential medium (MEM, ThermoFisher Scientific). For cultivation of optogenetic MDCK cells, selective antibiotics (1.0 $\mu\text{g mL}^{-1}$ puromycin, 80 $\mu\text{g mL}^{-1}$ G418, 10 $\mu\text{g mL}^{-1}$ zeocin, and 1.0 $\mu\text{g mL}^{-1}$ blasticidin S.) were added in the MEM. For time-lapse imaging, the MDCK cells were placed on a glass base dish ($\phi=35$ mm, IWAKI,

3000-035) with a channel-shaped pattern 500 μm in width with MPC polymer (Lipidure-CM5206, NOF Corporation) on its surface. Figures 4 and 5 show the wound healing assay. We cultured the cell population in a two-well culture insert (ibidi, 81176) and then removed the culture insert when the density reached the confluent level. Microscopic observation was started at the time of removal, and time $t = 0$ was defined as 8 hours after removal of the culture insert. The propagation of ERK waves was observed at a distance of at least 500 μm from the area where the wound was formed.

B. Quantitative analysis

We performed fluorescent labeling of the cell nucleus at each time point in the time-lapse measurement, and the velocity of cell migration was determined by calculating the distance traveled per unit time of the cell nucleus. The orientation angle in the cell monolayer at position \mathbf{x} , defined as $\theta(\mathbf{x})$, was calculated from bright-field images using OrientationJ in the Fiji plugin, with the window size set to 0.75 μm and the gradient type set to cubic spline. The orientation angle was then analyzed by calculating the orientation order parameter of a two-dimensional system, $S = \sqrt{\langle \cos 2\theta \rangle_{ROI}^2 + \langle \sin 2\theta \rangle_{ROI}^2}$ within a region of interest (ROI) of size $w = 50 \mu\text{m}$. S is a scalar order parameter used to analyze the signal-dependent change of the orientation field.

We evaluated the signaling activity of ERK MAP kinase by recording the translocation of ERK-mCherry into

the nucleus. We recorded the fluorescence intensities of ERK-mCherry inside and outside the nucleus, C_{in} and C_{out} , respectively. We then defined the ERK signal E as

$$E = \frac{C_{in}}{C_{out}}. \quad (29)$$

The activated ERK signal was calculated as $\Delta E = E - E_0$, where E_0 is the ERK signal at basal conditions (the absence of blue laser illumination).

We analyzed the dynamics of migration speed, density change and orientation change at the location of interest (labeled with **a**, **b**, **c**, **d**) as the ERK wave propagates. The cross-correlation functions between ERK activity and migration velocity ($C_u(\Delta t)$), ERK activity and local cell density ($C_\rho(\Delta t)$), and ERK activity and orientation order ($C_S(\Delta t)$), which appeared in Fig. 4, are defined as follows

$$C_u(\Delta t) = \frac{\langle (\Delta E(t) - \overline{\Delta E})(u_x(t + \Delta t) - \overline{u_x}) \rangle_t}{\langle (\Delta E(t) - \overline{\Delta E})(u_x(t) - \overline{u_x}) \rangle_t}$$

$$C_\rho(\Delta t) = \frac{\langle (\Delta E(t) - \overline{\Delta E})(\rho(t + \Delta t) - \overline{\rho}) \rangle_t}{\langle (\Delta E(t) - \overline{\Delta E})(\rho(t) - \overline{\rho}) \rangle_t}$$

$$C_S(\Delta t) = \frac{\langle (\Delta E(t) - \overline{\Delta E})(S(t + \Delta t) - \overline{S}) \rangle_t}{\langle (\Delta E(t) - \overline{\Delta E})(S(t) - \overline{S}) \rangle_t}$$

where $\overline{\Delta E}$, $\overline{u_x}$, $\overline{\rho}$, \overline{S} are the average of ERK activity, migration speed against the direction of the ERK wave propagation, local cell density, and orientation order parameter, respectively. $\langle \cdot \rangle$ is the ensemble average over time. In Figure 4, the cross-correlation function is calculated at four locations, and the average is plotted as a solid line, with the standard deviation shown as a light-colored area.

-
- [1] P. Friedl and D. Gilmour, Collective cell migration in morphogenesis, regeneration and cancer, *Nature Reviews Molecular Cell Biology* **10**, 445 (2009).
- [2] Y. Matsubayashi, M. Ebisuya, S. Honjoh, and E. Nishida, Erk activation propagates in epithelial cell sheets and regulates their migration during wound healing, *Current Biology* **14**, 731 (2004).
- [3] K. Aoki, Y. Kumagai, A. Sakurai, N. Komatsu, Y. Fujita, C. Shionyu, and M. Matsuda, Stochastic erk activation induced by noise and cell-to-cell propagation regulates cell density-dependent proliferation, *Molecular Cell* **52**, 529 (2013).
- [4] T. Hiratsuka, Y. Fujita, H. Naoki, K. Aoki, Y. Kamioka, and M. Matsuda, Intercellular propagation of extracellular signal-regulated kinase activation revealed by in vivo imaging of mouse skin, *eLife* **4**, e05178 (2015).
- [5] K. Aoki, Y. Kondo, H. Naoki, T. Hiratsuka, R. E. Itoh, and M. Matsuda, Propagating wave of erk activation orients collective cell migration, *Developmental Cell* **43**, 305–317.e5 (2017).
- [6] C. J. Weijer, Collective cell migration in development, *Journal of Cell Science* **122**, 3215 (2009).
- [7] R. Seger and E. G. Krebs, The mapk signaling cascade, *The FASEB journal* **9**, 726 (1995).
- [8] C. Londono, M. J. Loureiro, B. Slater, P. B. Lucker, J. Soleas, S. Sathanathan, J. S. Aitchison, A. J. Kabla, and A. P. McGuigan, Nonautonomous contact guidance signaling during collective cell migration, *Proceedings of the National Academy of Sciences USA* **111**, 1807 (2014).
- [9] E. M. Purcell, Life at low reynolds number, *American Journal of Physics* **45**, 3 (1977).
- [10] A. Najafi and R. Golestanian, Simple swimmer at low reynolds number: Three linked spheres, *Physical Review E* **69**, 062901 (2004).
- [11] C. Lozano and C. Bechinger, Diffusing wave paradox of phototactic particles in traveling light pulses, *Nature Communications* **10**, 2495 (2019).
- [12] K. V. Kumar, S. Ramaswamy, and M. Rao, Active elastic dimers: Self-propulsion and current reversal on a featureless track, *Physical Review E* **77**, 020102 (2008).
- [13] T. Qiu, T.-C. Lee, A. G. Mark, K. I. Morozov, R. Münster, O. Mierka, S. Turek, A. M. Leshansky, and P. Fischer, Swimming by reciprocal motion at low reynolds number, *Nature Communications* **5**, 5119 (2014).
- [14] E. Lauga, Life around the scallop theorem, *Soft Matter*

- 7, 3060 (2011).
- [15] M. Leoni and P. Sens, Model of cell crawling controlled by mechanosensitive adhesion, *Physical Review Letters* **118**, 228101 (2017).
- [16] M. H. Mai and B. A. Camley, Hydrodynamic effects on the motility of crawling eukaryotic cells, *Soft Matter* **16**, 1349 (2020).
- [17] S. Garcia, E. Hannezo, J. Elgeti, J.-F. Joanny, P. Silberzan, and N. S. Gov, Physics of active jamming during collective cellular motion in a monolayer, *Proceedings of the National Academy of Sciences* **112**, 15314 (2015).
- [18] C. Blanch-Mercader, V. Yashunsky, S. Garcia, G. Duclos, L. Giomi, and P. Silberzan, Turbulent dynamics of epithelial cell cultures, *Physical Review Letters* **120**, 208101 (2018).
- [19] R. Mueller, J. M. Yeomans, and A. Doostmohammadi, Emergence of active nematic behavior in monolayers of isotropic cells, *Physical Review Letters* **122**, 048004 (2019).
- [20] S.-Z. Lin, W.-Y. Zhang, D. Bi, B. Li, and X.-Q. Feng, Energetics of mesoscale cell turbulence in two-dimensional monolayers, *Communications Physics* **4**, 21 (2021).
- [21] C. Pérez-González, G. Ceada, F. Greco, M. Matejčić, M. Gómez-González, N. Castro, A. Menendez, S. Kale, D. Krndjija, A. G. Clark, *et al.*, Mechanical compartmentalization of the intestinal organoid enables crypt folding and collective cell migration, *Nature cell biology* **23**, 745 (2021).
- [22] T. Brandstätter, D. B. Brückner, Y. L. Han, R. Alert, M. Guo, and C. P. Broedersz, Curvature induces active velocity waves in rotating spherical tissues, *Nature Communications* **14**, 1643 (2023).
- [23] T. Nagai and H. Honda, A dynamic cell model for the formation of epithelial tissues, *Philosophical Magazine B* **81**, 699 (2001).
- [24] A. G. Fletcher, M. Osterfield, R. E. Baker, and S. Y. Shvartsman, Vertex models of epithelial morphogenesis, *Biophysical Journal* **106**, 2291 (2014).
- [25] D. L. Barton, S. Henkes, C. J. Weijer, and R. Sknepnek, Active vertex model for cell-resolution description of epithelial tissue mechanics, *PLoS Computational Biology* **13**, e1005569 (2017).
- [26] S.-Z. Lin, S. Ye, G.-K. Xu, B. Li, and X.-Q. Feng, Dynamic migration modes of collective cells, *Biophysical Journal* **115**, 1826 (2018).
- [27] See Supplemental Material at <http://link.aps.org/supplemental/> for experimental materials and methods, for a detailed description of theoretical calculation.
- [28] S. Wang and P. G. Wolynes, On the spontaneous collective motion of active matter, *Proceedings of the National Academy of Sciences USA* **108**, 15184 (2011).
- [29] H. Tanimoto and M. Sano, A simple force-motion relation for migrating cells revealed by multipole analysis of traction stress, *Biophysical Journal* **106**, 16 (2014).
- [30] H. Ebata, K. Moriyama, T. Kuboki, and S. Kidoaki, General cellular durotaxis induced with cell-scale heterogeneity of matrix-elasticity, *Biomaterials* **230**, 119647 (2020).
- [31] M. Tarama and R. Yamamoto, Mechanics of cell crawling by means of force-free cyclic motion, *Journal of the Physical Society of Japan* **87**, 044803 (2018).
- [32] F. M. Weinert, J. A. Kraus, T. Franosch, and D. Braun, Microscale fluid flow induced by thermoviscous expansion along a traveling wave, *Physical Review Letters* **100**, 164501 (2008).
- [33] T. Fukuyama, S. Nakama, and Y. T. Maeda, Thermal molecular focusing: tunable cross effect of phoresis and light-driven hydrodynamic focusing, *Soft Matter* **14**, 5519 (2018).
- [34] S. Banerjee, K. J. Utuje, and M. C. Marchetti, Propagating stress waves during epithelial expansion, *Physical Review Letters* **114**, 228101 (2015).
- [35] S. Yabunaka and P. Marcq, Emergence of epithelial cell density waves, *Soft Matter* **13**, 7046 (2017).
- [36] Y. Asakura, Y. Kondo, K. Aoki, and H. Naoki, Hierarchical modeling of mechano-chemical dynamics of epithelial sheets across cells and tissue, *Scientific Reports* **11**, 4069 (2021).
- [37] T. B. Saw, A. Doostmohammadi, V. Nier, L. Kocgozlu, S. Thampi, Y. Toyama, P. Marcq, C. T. Lim, J. M. Yeomans, and B. Ladoux, Topological defects in epithelia govern cell death and extrusion, *Nature* **544**, 212 (2017).
- [38] K. Kawaguchi, R. Kageyama, and M. Sano, Topological defects control collective dynamics in neural progenitor cell cultures, *Nature* **545**, 327 (2017).
- [39] A. Doostmohammadi, J. Ignés-Mullol, J. M. Yeomans, and F. Sagués, Active nematics, *Nature Communications* **9**, 3246 (2018).
- [40] A. Saraswathibhatla, J. Zhang, and J. Notbohm, Coordination of contractile tension and cell area changes in an epithelial cell monolayer, *Physical Review E* **105**, 024404 (2022).
- [41] J.-M. Yang, S. Bhattacharya, H. West-Foyle, C.-F. Hung, T.-C. Wu, P. A. Iglesias, and C.-H. Huang, Integrating chemical and mechanical signals through dynamic coupling between cellular protrusions and pulsed erk activation, *Nature Communications* **9**, 4673 (2018).
- [42] N. Hino, L. Rossetti, A. Marín-Llauradó, K. Aoki, X. Trepát, M. Matsuda, and T. Hirashima, Erk-mediated mechanochemical waves direct collective cell polarization, *Developmental Cell* **53**, 646 (2020).
- [43] A. Ueki and S. Kidoaki, Manipulation of cell mechanotaxis by designing curvature of the elasticity boundary on hydrogel matrix, *Biomaterials* **41**, 45 (2015).
- [44] L. Balasubramaniam, A. Doostmohammadi, T. B. Saw, G. H. N. S. Narayana, R. Mueller, T. Dang, M. Thomas, S. Gupta, S. Sonam, A. S. Yap, *et al.*, Investigating the nature of active forces in tissues reveals how contractile cells can form extensile monolayers, *Nature Materials* **20**, 1156 (2021).
- [45] K. Shigeta, T. Fukuyama, R. Takahashi, K. Beppu, A. Tanaka, and Y. T. Maeda, Collective motion of epithelial cells along a wrinkled 3d-buckled hydrogel, *RSC Advances* **12**, 20174 (2022).
- [46] K. V. Iyer, R. Piscitello-Gómez, J. Pajmans, F. Jülicher, and S. Eaton, Epithelial viscoelasticity is regulated by mechanosensitive e-cadherin turnover, *Current Biology* **29**, 578 (2019).
- [47] A. Hamadi, M. Bouali, M. Dontenwill, H. Stoeckel, K. Takeda, and P. Ronde, Regulation of focal adhesion dynamics and disassembly by phosphorylation of fak at tyrosine 397, *Journal of Cell Science* **118**, 4415 (2005).
- [48] A. Zaritsky, D. Kaplan, I. Hecht, S. Natan, L. Wolf, N. S. Gov, E. Ben-Jacob, and I. Tsarfaty, Propagating waves of directionality and coordination orchestrate collective cell migration, *PLOS Computational Biology* **10**, 1 (2014).
- [49] M. Basan, J. Elgeti, E. Hannezo, W.-J. Rappel, and H. Levine, Alignment of cellular motility forces with tis-

- sue flow as a mechanism for efficient wound healing, *Proceedings of the National Academy of Sciences USA* **110**, 2452 (2013).
- [50] A. Brugués, E. Anon, V. Conte, J. H. Veldhuis, M. Gupta, J. Colombelli, J. J. Muñoz, G. W. Brodland, B. Ladoux, and X. Trepat, Forces driving epithelial wound healing, *Nature Physics* **10**, 683 (2014).
- [51] R. J. Tetley, M. F. Staddon, D. Heller, A. Hoppe, S. Banerjee, and Y. Mao, Tissue fluidity promotes epithelial wound healing, *Nature Physics* **15**, 1195 (2019).
- [52] D. Boocock, N. Hino, N. Ruzickova, T. Hirashima, and E. Hannezo, Theory of mechanochemical patterning and optimal migration in cell monolayers, *Nature Physics* **17**, 267 (2021).
- [53] D. Boocock, T. Hirashima, and E. Hannezo, Interplay between mechanochemical patterning and glassy dynamics in cellular monolayers, *PRX Life* **1**, 013001 (2023).
- [54] S. Tlili, M. Durande, C. Gay, B. Ladoux, F. Graner, and H. Delanoë-Ayari, Migrating epithelial monolayer flows like a maxwell viscoelastic liquid, *Physical Review Letters* **125**, 088102 (2020).
- [55] H. Y. Yoshikawa, F. F. Rossetti, S. Kaufmann, T. Kaindl, J. Madsen, U. Engel, A. L. Lewis, S. P. Armes, and M. Tanaka, Quantitative evaluation of mechanosensing of cells on dynamically tunable hydrogels, *Journal of the American Chemical Society* **133**, 1367 (2011).
- [56] L. Yu, J. Li, J. Hong, Y. Takashima, N. Fujimoto, M. Nakajima, A. Yamamoto, X. Dong, Y. Dang, Y. Hou, *et al.*, Low cell-matrix adhesion reveals two subtypes of human pluripotent stem cells, *Stem Cell Reports* **11**, 142 (2018).
- [57] S. Jain, V. M. Cachoux, G. H. Narayana, S. de Beco, J. D'alessandro, V. Cellerin, T. Chen, M. L. Heuzé, P. Marcq, R.-M. Mège, *et al.*, The role of single-cell mechanical behaviour and polarity in driving collective cell migration, *Nature Physics* **16**, 802 (2020).
- [58] K. E. Cavanaugh, M. F. Staddon, T. A. Chmiel, R. Harmon, S. Budnar, A. S. Yap, S. Banerjee, and M. L. Gardel, Force-dependent intercellular adhesion strengthening underlies asymmetric adherens junction contraction, *Current Biology* **32**, 1986 (2022).
- [59] P. Guillamat, C. Blanch-Mercader, G. Pernellet, K. Kruse, and A. Roux, Integer topological defects organize stresses driving tissue morphogenesis, *Nature Materials* **21**, 588 (2022).
- [60] M. Deforet, V. Hakim, H. G. Yevick, G. Duclos, and P. Silberzan, Emergence of collective modes and tridimensional structures from epithelial confinement, *Nature Communications* **5**, 3747 (2014).
- [61] R. Ienaga, K. Beppu, and Y. T. Maeda, Geometric confinement guides topological defect pairings and emergent flow in nematic cell populations, *Soft Matter* **19**, 5016 (2023).
- [62] P. A. Gagliardi, M. Dobrzyński, M.-A. Jacques, C. Dessauges, P. Ender, Y. Blum, R. M. Hughes, A. R. Cohen, and O. Pertz, Collective erk/akt activity waves orchestrate epithelial homeostasis by driving apoptosis-induced survival, *Developmental Cell* **56**, 1712 (2021).
- [63] A. De Simone, M. N. Evanitsky, L. Hayden, B. D. Cox, J. Wang, V. A. Tornini, J. Ou, A. Chao, K. D. Poss, and S. Di Talia, Control of osteoblast regeneration by a train of erk activity waves, *Nature* **590**, 129 (2021).